JCB Article

Direct measurement of Gag–Gag interaction during retrovirus assembly with FRET and fluorescence correlation spectroscopy

Daniel R. Larson,[1] Yu May Ma,[2] Volker M. Vogt,[2] and Watt W. Webb[1]

[1]School of Applied and Engineering Physics and [2]Department of Molecular Biology and Genetics, Cornell University, Ithaca, NY 14853

During retrovirus assembly, the polyprotein Gag directs protein multimerization, membrane binding, and RNA packaging. It is unknown whether assembly initiates through Gag–Gag interactions in the cytosol or at the plasma membrane. We used two fluorescence techniques—two-photon fluorescence resonance energy transfer and fluorescence correlation spectroscopy—to examine Rous sarcoma virus Gag–Gag and –membrane interactions in living cells. Both techniques provide strong evidence for interactions between Gag proteins in the cytoplasm. Fluorescence correlation spectroscopy measurements of mobility suggest that Gag is present in large cytosolic complexes, but these complexes are not entirely composed of Gag. Deletion of the nucleocapsid domain abolishes Gag interactions and membrane targeting. Deletion of the membrane-binding domain leads to enhanced cytosolic interactions. These results indicate that Gag–Gag interactions occur in the cytosol, are mediated by nucleocapsid domain, and are necessary for membrane targeting and budding. These methods also have general applicability to in vivo studies of protein–protein and –membrane interactions involved in the formation of complex macromolecular structures.

Introduction

The multi-step process of retrovirus assembly is a paradigm for a range of cellular macromolecular interactions and involves protein–protein, –membrane, and –nucleic acid interactions. The retrovirus polyprotein Gag directs assembly and is the only viral protein required for formation, budding, and release of virus-like particles (VLPs) from the plasma membrane (Wills and Craven, 1991; Gottlinger, 2001). Late in the budding process, Gag is cleaved into at least three proteins common to all retroviruses: the matrix domain (MA) is responsible for membrane targeting; the capsid domain (CA) forms the shell of the mature viral core; and the nucleocapsid domain (NC) is an RNA binding protein, which incorporates the genomic RNA into the virus. During assembly, patches of aggregated Gag proteins associated with the inner face of the plasma membrane appear to enlarge, curving outwards to form buds that eventually pinch off from the cell (Craven and Parent, 1996). It is unknown whether molecules of Gag become inserted individually into the polymerizing protein shell on the membrane, or if Gag molecules form oligomeric intermediates in the cytoplasm, which then are transported to membrane assembly sites. Three pieces of evidence suggest that membrane binding is not the prerequisite for Gag–Gag interaction. First, Gag molecules defective in membrane binding can be rescued into budding particles by coexpression of wild-type Gag (Wills et al., 1991; Morikawa et al., 1996). Second, HIV-1 MA is reported to bind to membranes in vitro less efficiently than full-length Gag, suggesting a cooperative role for Gag multimerization in this process (Zhou and Resh, 1996; Sandefur et al., 1998). Third, purified Gag proteins or fragments of Gag spontaneously form VLPs in vitro in the absence of membrane, implying that Gag proteins have inherent ability to multimerize at appropriate concentrations (Klikova et al., 1995; Campbell and Vogt, 1997; Gross et al., 1997; von Schwedler et al., 1998; Campbell and Rein, 1999). Despite these observations, Gag–Gag interaction in the cytoplasm of living cells has not been demonstrated.

Address correspondence to Watt W. Webb, 212 Clark Hall, Cornell University School of Applied and Engineering Physics, Ithaca, NY 14853. Tel.: (607) 255-3331. Fax: (607) 255-7658. email: www2@cornell.edu

M. Ma's present address is Dept. of Cell Biology, Harvard Medical School, Boston, MA 02115.

Key words: Rous sarcoma virus; two photon; fluorescence resonance energy transfer; protein–protein transfer

Abbreviations used in this paper: 2PE, 2-photon excitation; CA, capsid domain; FCS, fluorescence correlation spectroscopy; FRET, fluorescence resonance energy transfer; MA, matrix domain; NC, nucleocapsid domain; PR, protease domain; RSV, Rous sarcoma virus; VLP, virus-like particle.

Here, we use two fluorescence-based methods using 2-photon excitation (2PE; Denk et al., 1990) to address the extent and spatial location of interactions between Gag molecules in living cells. The first is fluorescence resonance energy transfer (FRET), between donor and acceptor fluorophores tagged to two different molecules of Gag. The rate of energy transfer depends on the inverse sixth power of the distance between donor and acceptor, so FRET can be used to probe distances on the order of 5 nm (Periasamy, 2001; Sekar and Periasamy, 2003). The second method is fluorescence correlation spectroscopy (FCS; Magde et al., 1972; Elson and Magde, 1974). FCS provides dynamic information on fluorescent fluctuations and can be used to measure diffusion and concentration of fluorescent species (Thompson, 1991; Hess et al., 2002). Diffusion coefficients measured by FCS are used to calculate approximate sizes of Gag-containing complexes in cells, and quantification of the fluorescence intensity of the diffusing complex is used to estimate the number of Gag molecules in the complex. FRET and FCS are complementary techniques in that FRET is sensitive to the distance between donor and acceptor, and FCS provides information about the size of complexes and their interaction with the cellular environment.

We describe the implementation of 2PE FCS and FRET for studying Rous sarcoma virus (RSV) Gag–Gag interactions in living cells. FRET measurements indicate that direct Gag–Gag interactions occur not only at the plasma membrane but also in the cytoplasm, suggesting that the plasma membrane is not necessary for the initial steps of RSV assembly. FCS measurements reveal that most Gag molecules exist in the cytoplasm as part of large complexes. Deletion of the NC abolishes all Gag–Gag interactions. These results indicate that cytosolic Gag–Gag interactions are necessary for membrane binding and budding and are mediated by NC-RNA binding. The methods developed here should have utility for studying a wide array of cell biological problems involving assembly of complex supermolecular structures.

Results

Gag-GFP behaves similarly to wt Gag

We used a previously described RSV Gag-GFP fusion protein in which the last six amino acid residues of NC and the entire protease domain (PR) are replaced by GFP (Fig. 1 A). This protein gives rise to morphologically normal budding VLPs in COS1 cells (Callahan and Wills, 2000). Then, we constructed parallel plasmids in which the GFP coding sequence was replaced by that of CFP or YFP. To verify that the expression level and budding efficiency of the chimeric proteins was similar to that of Gag, we created two Gag constructs lacking foreign sequences. GagD37S contains an active site mutation in the PR, and GagΔPR lacks the PR entirely (Fig. 1 A). DF-1 cells were pulse labeled with [^{35}S]methionine and chased for 1 h. All three proteins, GagD37S, GagΔPR, and Gag-GFP, were found in undegraded form in cell lysates by immunoprecipitation with anti-Gag antiserum (Fig. 1 B). At this chase time, about one half of the protein was present as particles in the medium (Fig. 1 B), and the density was that of normal retroviruses, 1.17 g/ml in an equilibrium sucrose density gradient. In cells expressing Gag-GFP, this was the only protein in cell lysates that was recognized by anti-GFP antiserum, ensuring that the fluorescence observed in the transfected cells could be attributed to Gag-GFP (Fig. 1 B).

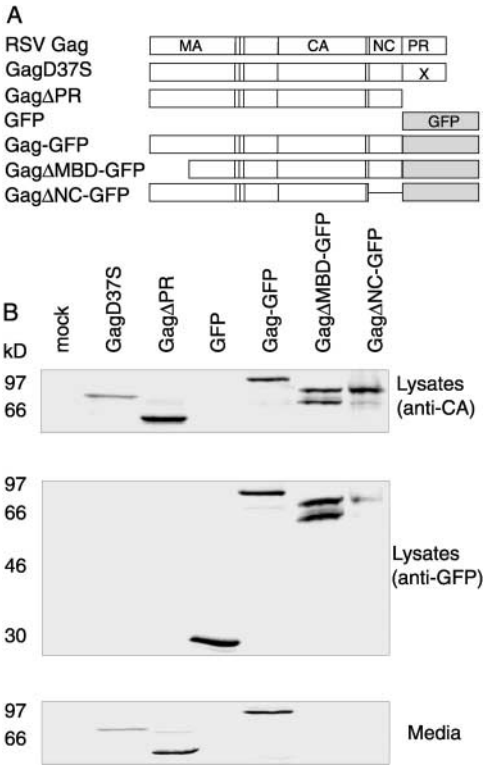

Figure 1. **Expression and assembly of RSV Gag proteins.** (A) Schematic diagram of proteins. The wild-type Gag protein with its major domains is shown on the top line. Vertical lines denote cleavage sites for the viral protease. All DNAs were expressed in transiently transfected cells from a CMV promoter. Three versions of each fluorescent chimeric protein were built (GFP, CFP, and YFP). (B) Expression and budding. Transfected DF-1 cells were pulse labeled with [^{35}S]methionine and chased for 1 h. The proteins in cell lysates were immunoprecipitated with anti-CA antiserum (top) or anti-GFP antiserum (middle). The medium from each plate of cells was centrifuged to collect the shed VLPs.

To further assess the fidelity of the chimeric fluorescent protein as a model for Gag, we compared the budding rate of Gag-GFP with that of GagD37S. Transfected cells were pulse labeled and chased for different times, and the amounts of Gag-GFP and GagD37S were determined in the medium after collection of VLPs, and in the cells after immunoprecipitation of lysates. Progressively more of the proteins appeared in the medium at longer chase times (Fig. 2 A, lanes V compared with lanes C). Quantification of this and similar experiments showed that the half-time of budding was similar for the two proteins, ~0.5–1 h, although the Gag protein appeared to bud slightly faster than the chimeric Gag-GFP (Fig. 2 B). The observation that the sum of all protein in both medium and cells was constant with time implies that the majority of newly synthesized RSV Gag and Gag-GFP protein is not subject to degradation. Together, the results in Figs. 1 and 2 suggest that Gag-GFP is suitable as a model protein for studies of assembly in vivo by fluorescence techniques.

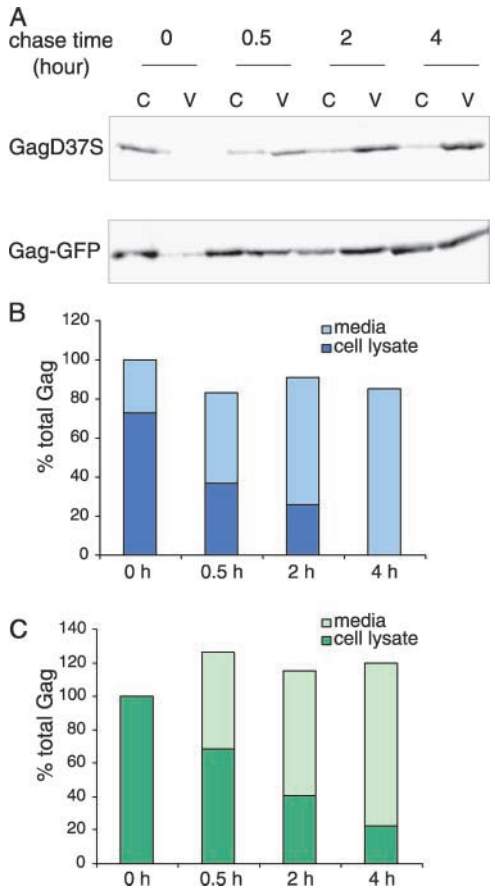

Figure 2. **Budding kinetics of Gag proteins.** Separate dishes of DF-1 cells transfected with DNAs expressing GagD37S or Gag-GFP were pulse labeled for 10 min with [^{35}S]methionine, and then chased in cold medium for 0.5, 2, or 4 h. (A) The labeled Gag protein remaining in the cells (C) was visualized after immunoprecipitation with anti-CA serum, and the amount of labeled Gag in VLPs (V) was visualized after collection of the particles by centrifugation. (B and C) Quantitation of the labeled Gag bands from A. The total Gag (V + C) in the pulse label was set to 100%.

Visualization of wt and mutant Gag-GFPs

We visualized cells cotransfected with two plasmids, one encoding a donor (CFP) and the other an acceptor (YFP) fluorescent protein, either as fusions with Gag or without added viral sequences. The free proteins CFP/YFP showed diffuse and homogeneous staining over the cytoplasm and nucleus (Fig. 3 A). As expected from the absence of predicted protein–protein interactions in this case, the cyan channel was brighter, with the yellow channel representing bleed-through, i.e., emission of the donor at the longer wavelength. The fluorescence pattern of Gag-CFP/Gag-YFP was markedly different, showing strong punctate staining. The bright spots at the plasma membrane are presumably sites of virus assembly (Fig. 3 B). Fluorescent particles released from the cells also could be seen diffusing in the media and adhering to the coverslip.

We constructed two pairs of Gag-CFP/Gag-YFP deletion mutants that abolish assembly in known ways. GagΔMBD lacks the membrane-binding domain, and cannot form budding structures (Fig. 1 A; Callahan and Wills, 2000). Cells cotransfected with plasmids encoding GagΔMBD-CFP and GagΔMBD-YFP showed large fluorescent aggregates throughout the cytoplasm (Fig. 3 C). The aggregates were macroscopic (>2 μm), in contrast to the sub-resolution spots formed by wild-type Gag (Hermida-Matsumoto and Resh, 2000). As expected, no particles were observed in the medium or adhered to the coverslip, because budding was abolished.

The second pair of mutant Gag constructs, GagΔNC-CFP and GagΔNC-YFP, lack NC. When coexpressed these constructs gave rise to diffuse homogeneous staining (Fig. 3 D), similar to that observed in cells expressing free CFP and YFP. No punctate features were evident and the plasma

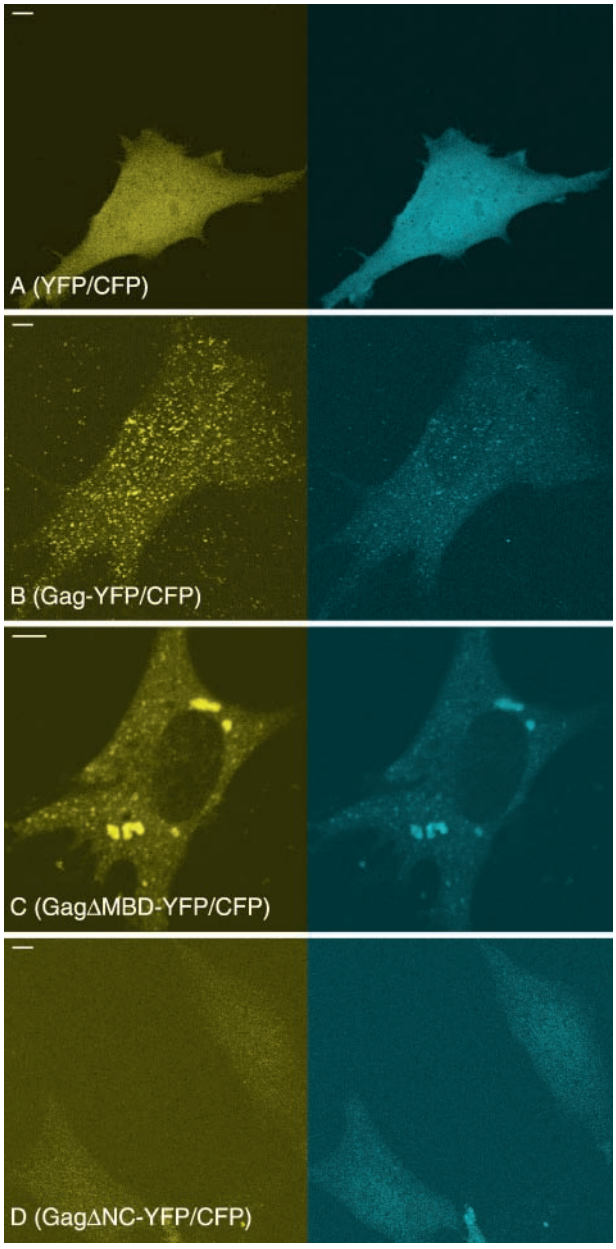

Figure 3. **Two-photon laser scanning microscopy images of transiently transfected DF-1 cells.** A is control cells; B is wt Gag; C is ΔMBD Gag; and D is ΔNC Gag. Each set of images of a single cell is composed of the yellow and cyan channel. Bar, 5 μm. Excitation, 830 nm at 4 mW.

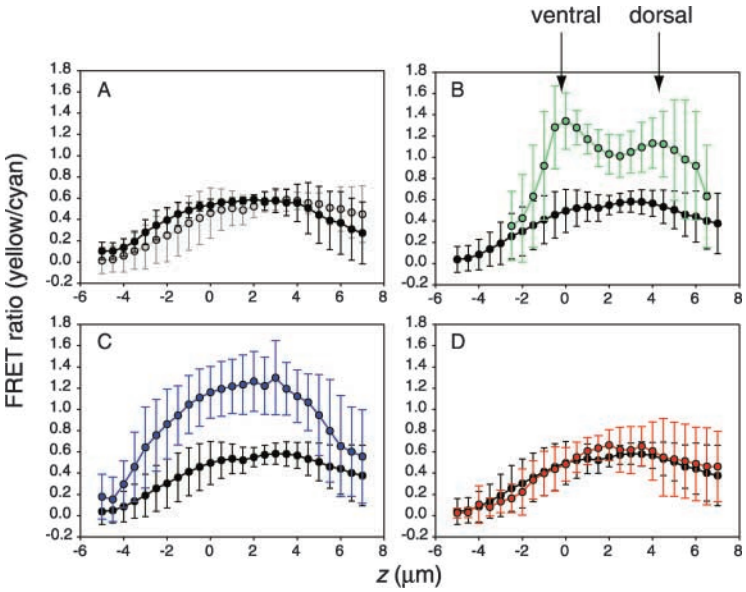

Figure 4. **z-series FRET measurements.** Each point in the curve corresponds to the ratio of yellow to blue as described in the methods section. The step size in z is 0.5 μm, with the zero position chosen to be contact plane of the ventral surface of the cells with the coverslip. Negative values correspond to distances below the coverslip (outside the dish); positive values correspond to positions above the coverslip (inside the dish). A shows control curves. The black circles represent cells expressing CFP or Gag-CFP (n = 11 cells), and the gray circles represent cells coexpressing CFP and YFP (n = 6 cells). These curves were then averaged to obtain the control curve for the other panels. B shows the same type of analysis for cells coexpressing Gag-CFP and Gag-YFP (n = 11 cells), C for cells coexpressing GagΔMBD-CFP and GagΔMBD-YFP (n = 5 cells), and D for cells coexpressing GagΔNC-CFP and GagΔNC-YFP (n = 13 cells). The error bars are the measured SEM.

membrane showed no enhanced staining. Moreover, unlike the wild-type Gag and the mutant GagΔMBD chimeric proteins, GagΔNC-CFP/GagΔNC-YFP fluorescence was not excluded from the nucleus.

Cytosolic Gag–Gag interactions measured by FRET

The VLPs in the process of budding from the plasma membrane provide a positive control for FRET. The particles, when completely formed, are expected to contain ~1,500 copies of chimeric Gag (Vogt and Simon, 1999) in a sphere with an external diameter of 125 nm (Kingston et al., 2001), with the CFP or YFP domains located in the central portion of the VLP, in a volume of $\sim 10^5$ nm^3 (Yu et al., 2001). Thus the CFP and YFP domains approach closest packing and extensive energy transfer is expected. The negative control for FRET comes from the cells coexpressing free CFP and YFP (Fig. 3 A), which accounts both for CFP emission bleedthrough into the yellow channel and for direct excitation of the YFP.

FRET analysis was applied to stacks of images acquired at 0.5-μm intervals throughout the cells. The vertical dimension of the focal volume in which 2PE occurs is ~1.2 μm, and, thus, molecules excited in this volume will be scored in at most three z sections. Control cells expressing either free CFP or Gag-CFP (Fig. 4 A, black circles) or coexpressing free CFP and YFP (Fig. 4 A, gray circles) showed similar apparent FRET ratios, implying that CFP bleedthrough into the YFP channel is dominant. In all plots, negative x axis values correspond to z positions below the coverslip, and positive values are above the coverslip. The apparent FRET ratios increased for z sections moving from below the coverslip into the plane of the cells. This slow rise is due primarily to the thresholding procedure of the algorithm. Because only nonzero values of the cyan counts are valid in the denominator, when there is little fluorescence in both channels, as would be true below and above the cell, there are more pixels with cyan counts above threshold than pixels with yellow counts above threshold, leading to an apparent low FRET ratio. In addition, due to low light levels and mechanical and biological differences in the positions of the ventral and dorsal surfaces of multiple cells, the regions below and above the cell layer tend to be noisy, as reflected in the error bars. In sections through the cell (0 μm < z < 5 μm), there were many more counts, thresholding levels were unimportant, and the ratio was much more robust.

Bleedthrough from the cyan into the yellow channel gave an apparent maximum FRET ratio of 0.6 ± 10% (Fig. 4 A). This bleedthrough level and the accompanying error bars set the lower limit for detection of true FRET. The observation that there was no statistical difference between CFP alone and coexpressed CFP and YFP justifies our approach of using a single excitation: the bleedthrough background curve accounts adequately for CFP emission in the YFP channel and direct excitation of the YFP. The two curves in Fig. 4 A were averaged to yield the control curve displayed in subsequent FRET ratio plots.

The FRET ratios in cells coexpressing Gag-CFP and -YFP were dramatically higher than the ratios in cells expressing the control proteins (Fig. 4 B, green circles compared with black circles). The FRET ratio rose to a maximum at 0 μm, the position corresponding to the ventral surface. This peak reflects the putative sites of assembly and budding at the plasma membrane. The FRET ratio decreased in z sections through the middle of the cell but remained well above the control levels, implying energy transfer in the cytosolic regions of the cell that are dominated by cytoplasm instead of plasma membrane. As the z distance increased, the FRET ratio reached a second maximum, corresponding to the dorsal surface. Above the dorsal surface, the data became noisier due to low levels of fluorescence, and the ratio approached control levels. In conclusion, the height of the central trough over the control curve strongly suggests interactions between Gag-CFP and -YFP molecules in the cytoplasm.

Cytosolic Gag–Gag interactions are abolished by ΔNC but not by ΔMBD

We also performed the whole cell FRET analysis on cells expressing either of the two chimeric deletion mutants. For the

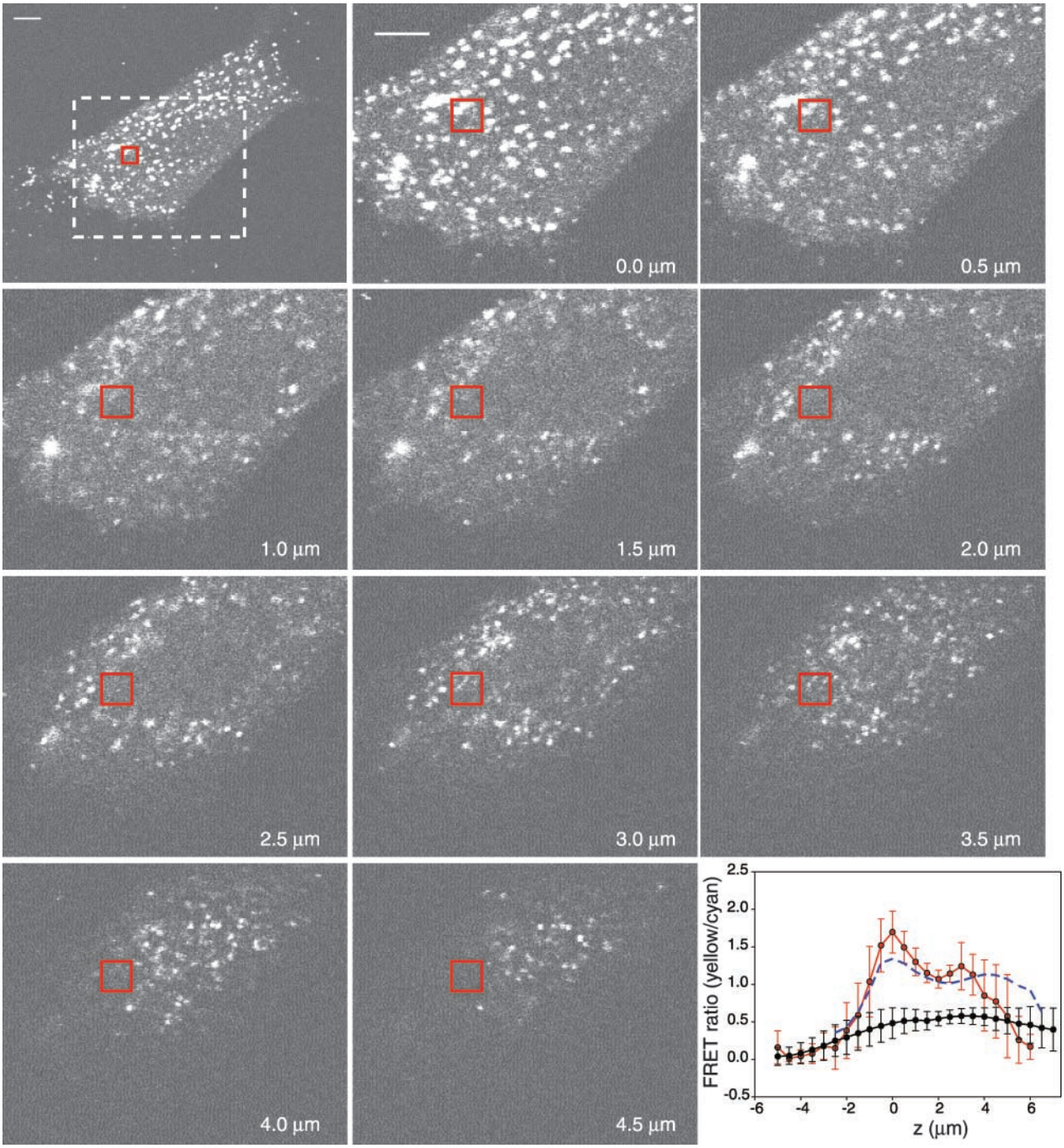

Figure 5. **z-series FRET measurements of regions within the cells.** The same analysis as described in Materials and methods is performed on a subsection of the images. The top left image is a full field image of a fibroblast at the ventral surface. Subsequent images are a 2× magnification of the region demarcated by a white dotted line. Bar, 5.0 µm. z position is denoted on each image. The analyzed region is demarcated by a red square and is the same region in each step of the z-series. The compiled results for 11 cells are shown in red in the plot at bottom right. The black line is the control, and the blue dotted line is the whole cell analysis. The error bars are the measured SEM.

pair of proteins GagΔMBD-CFP and GagΔMBD-YFP, which lack the membrane-binding domain, the bimodal FRET ratio was abolished and instead a single broad peak was evident (Fig. 4 C). These proteins become trapped inside the cell as large aggregates (Fig. 3 C) because they cannot undergo membrane association and budding. However, Gag–Gag interactions still occur, as evidenced by a high FRET ratio. Because GagΔMBD assembles into VLPs in vitro, it is possible that the macroscopic fluorescent aggregates represent clusters of such particles.

For the pair of proteins GagΔNC-CFP and GagΔNC-YFP, the FRET ratio was indistinguishable from control levels (Fig. 4 D), implying that Gag–Gag interactions were so sparse as to be below the limit of detectability. This result is consistent with previous reports that at least part of the NC is crucial for Gag assembly, and it also corroborates the find-

ing that the NC-nucleic acid binding is necessary for Gag dimerization in an in vitro assembly system with purified proteins (Ma and Vogt, 2002).

Gag–Gag interactions in regions lacking sites of assembly

The FRET ratios in Fig. 4 B are the result of whole-cell analyses in which the image information was killed to obtain a robust measurement of FRET at each z position in the cell. The interpretation of significant cytosolic FRET relies on the expectation that the cytosolic signal should dominate in the equatorial region of the cell. To confirm this expectation, we visually selected small centrally located regions in cells that appeared to be devoid of punctate staining (Fig. 5, red square). In the example shown, budding sites were clearly visible on the plasma membrane on the ventral surface (Fig. 5, z = 0.0 μm), but as the z distance increased these spots disappeared in the cytoplasm (Fig. 5, z = 2.0 μm), and then new spots appeared on the dorsal surface (Fig. 5, z = 3.5 μm).

The FRET ratios were determined by means of the same algorithm used for whole cells and were averaged over multiple cells (Fig. 5, bottom right, red circles). The criteria for selection of a region within the cell are that there be a punctate pattern on the ventral and dorsal surface but diffuse fluorescence in the middle of the cell. For comparison, the blue dotted line shows the result from the whole cell analysis from Fig. 4 B. Again, the trough of the curve near z = 2.0 μm was significantly above the control levels, indicating that extensive Gag–Gag interaction occurred even in the middle of the cell in the absence of any punctate pattern. The level of FRET in the inset agrees well with that determined for whole cells, especially at the ventral surface and in the trough, indicating that the plasma membrane contributions are minor in equatorial z positions. The difference between the position of the dorsal peak in the inset and that in whole cell is a consequence of the visual selection procedure. We chose inset regions to the side of the nucleus. In an adherent fibroblast the highest point in the cell is above the nucleus, and thus the dorsal plasma membrane in the inset z sections is expected to be below the highest point in the whole cell.

FCS reveals that Gag is part of large complexes in the cytosol

The second method that we have used to study Gag–Gag interactions in vivo is FCS. The GFP chimeras were first imaged, and then the beam was positioned for the FCS measurement in a region of the cell without obvious punctate features. Normalized representative FCS curves from four fluorescent samples are shown in Fig. 6.

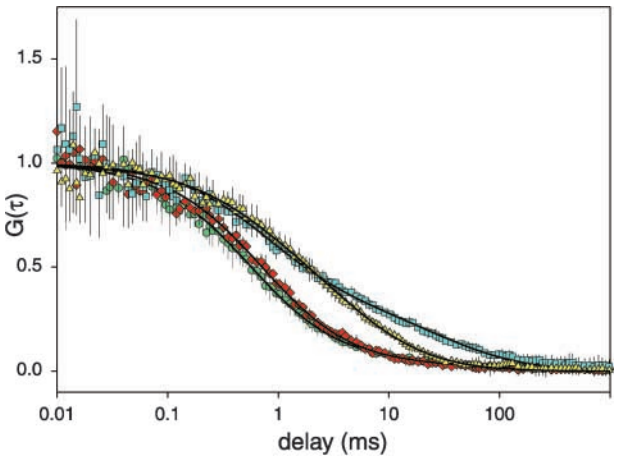

Figure 6. **Selected curves from intracellular FCS measurements on DF-1 cells.** G(τ) values are normalized to G(0) = 1 for display. Each curve is fit with four parameters: concentration (amplitude), two diffusion coefficients, and the relative fraction of the larger diffusion coefficient. The yellow triangles are Gag-GFP; the cyan squares are PM-GFP; the red diamonds are GagΔNC-GFP; and the green circles are GFP. Each curve is an average of five 10-s curves, and the error bars are the measured SD.

To fit these data (Fig. 6), we made the simplifying assumption that there were two diffusing species. This assumption is based on the known physiological function of Gag: one expects both membrane-bound and cytosolic fractions of the protein. Furthermore, the correlation measurements are not adequately described by simple, one-component diffusion. The diffusion coefficient of each species and the relative partition between species was calculated as described in the Materials and methods (second equation) and compiled in Table I. Two fluorescent molecules were used as controls for Gag-GFP. The first is free GFP itself, most of which is expected to be present in the cytosol and the nucleus (Chen et al., 2002). The second is PM-GFP, a version of GFP in which the NH_2-terminal sequence of the protein was engineered to carry both a myristoylation and a palmitoylation site, derived from the tyrosine kinase Lyn (Pyenta et al., 2001).

GFP showed one primary diffusion coefficient (D = 0.026 μm^2/ms, 95% fraction; Fig. 6, green circles), which is approximately fourfold lower than the diffusion coefficient in buffer (not depicted) and agrees with previously reported values (Dayel et al., 1999; Chen et al., 2002; Verkman,

Table I. **Diffusion coefficients for GFP chimeras**

Sample	D_1	D_2	Fraction of D_1
	μm^2/ms	μm^2/ms	
Gag-GFP	0.023 (0.005)	3.2×10^{-3} (6.4×10^{-4})	0.41
PM-GFP	0.019 (0.007)	4.8×10^{-4} (1.5×10^{-4})	0.66
GFP	0.026 (0.005)	1.7×10^{-4} (6.3×10^{-5})	0.95
GagΔNC-GFP	0.021 (0.004)	2.3×10^{-4} (7.6×10^{-5})	0.96

Fit parameters for representative FCS curves. D_1 is the fast diffusion component; D_2 is the slow diffusion component. The relative weights are included as the fraction of D_1. The SD is in parentheses.

2002). PM-GFP showed two diffusion coefficients, a fast component (D = 0.019 μm^2/ms, 66%) and a component that is two orders of magnitude slower (D = 4.8 × 10^{-4} μm^2/ms, 34%; Fig. 6, blue squares). The rapid component is similar in diffusion to cytosolic free GFP, and the slow component is characteristic of membrane-bound proteins (Niv et al., 1999). The cytosolic and the membrane components were easily resolvable, as seen in the difference between the two autocorrelation curves, again justifying the two-diffusion-component approach. It is important to note that the partitioning of PM-GFP between the membrane and cytoplasm (34% and 66%, respectively) reflects the total number of fluorescent molecules in the focal volume where excitation occurs, not the density of the molecules. If the focal volume cuts through the membrane, part of the contribution to the curve is from the cytosol and part is from the membrane. Even though the protein may have a higher density in the membrane, the larger volume of excitation that represents cytosol contributes significantly to the FCS measurement.

Gag-GFP (Fig. 6, yellow triangles) displayed diffusion properties intermediate between those of cytosolic (GFP) and membrane-bound (PM-GFP) proteins. The autocorrelation curve was fitted with a diffusion component corresponding to cytoplasmic diffusion (D = 0.023 μm^2/ms, 41%) and with a diffusion component, which is intermediate between cytoplasmic and membrane diffusion (D = 3.2 × 10^{-3} μm^2/ms, 59%). This component is an order of magnitude larger than membrane diffusion coefficients (D ≈10^{-4} μm^2/ms) and an order of magnitude smaller than cytosolic diffusion coefficients (D ≈10^{-2} μm^2/ms). Furthermore, using a two-component diffusion model, we observed this intermediate component alternately present with cytoplasmic and membrane diffusion components. We interpret this intermediate diffusion coefficient to represent Gag-containing complexes in the cytosol (see Discussion). The size of such complexes can be gauged only approximately from these data because the diffusion coefficient is relatively insensitive to molecular mass, being proportional to the inverse cube root of the mass for a fixed density. But in approximate terms for spherical particles, the observed 10-fold decrease in diffusion coefficient compared with free GFP would correspond to a particle of ~10–100 MD.

The appearance of the intermediate diffusing Gag-GFP component was dependent on presence of NC. Gag ΔNC-GFP showed a diffusion coefficient nearly identical to that of free GFP (D = 0.021 μm^2/ms, 96%) (Fig. 6, red diamonds). Thus, the NC is necessary for the formation of the large Gag-containing complexes, as well as for significant membrane association.

We generated a frequency plot of the diffusion coefficient distribution, compiled from many cells from separate experiments (Fig. 7). The x axis is the log of the diffusion coefficient (log[D]), and the y axis is the frequency of occurrence, weighted by the relative fraction measured in the FCS curve. The left side of the histograms corresponds to slow diffusion (coefficients with large negative exponents) and the right side to fast diffusion (coefficients with exponents approaching zero). GFP (Fig. 7 A) showed a sharp peak with the expected value for GFP diffusion in the cytoplasm. The lesser peaks are due to the small fraction of slow diffusing components (e.g., the 5% component of GFP in Table I) and also to the error inherent in diffusion measurements in living cells. PM-GFP (Fig. 7 B) showed a clearly bimodal distribution, with well-resolved peaks corresponding to the membrane and the cytosolic fractions. By contrast, Gag-GFP showed a broad distribution of diffusion coefficients with some values typical of the cytosol and of the membrane-bound components, but also a significant fraction with intermediate values (Fig. 7 C). Deletion of the NC collapsed this broad distribution to one more similar to that of free GFP (Fig. 7 D). Very little membrane diffusion was observed for GagΔNC-GFP, indicating that NC is required for Gag to become stably attached to the membrane under these conditions. One model to explain this result is that stable membrane association requires cooperative binding, which is mediated by NC. Formation of the large putative cytosolic complexes also was drastically diminished for GagΔNC-GFP, in agreement with the FRET result that no significant Gag–Gag interaction occurs for this mutant.

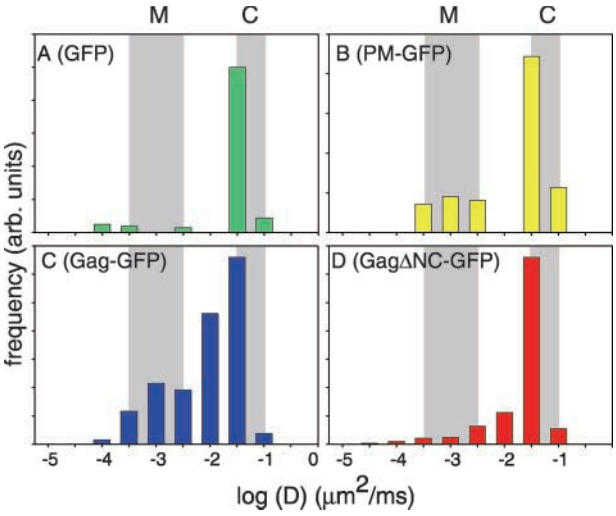

Figure 7. **Histogram of log (diffusion coefficient) for all cells.** Each FCS measurement in a cell yields two diffusion coefficients. The diffusion coefficients are weighted by their respective fractions and compiled into the above frequency plot. The minimum value is −5 (i.e., log(D) = −5, where D is in μm^2/ms); the maximum is 0; and the bin size is 0.5. M designates the diffusion peak of membrane associated species; and C designates the diffusion peak of cytosolic moieties. The number of cells for each construct is *n* = 16, 12, 17, and 19 for PM-GFP, GFP, Gag-GFP, and GagΔNC-GFP, respectively.

Intracellular complexes are not composed entirely of Gag

It is possible that the large Gag-GFP-containing complexes with intermediate diffusion coefficient might be sub-viral particles. In this case, a large number, probably hundreds, of Gag-GFP molecules would comprise the complex. To determine the extent of Gag–Gag interactions, we considered the relative brightness of each GFP chimera in cells. The amplitude of the autocorrelation provides the number of the diffusing species, and the average count rate is a measure of the photons collected from the focal volume. Therefore, one can obtain the count rate per molecule for each diffusing species. Furthermore, because the relative fraction of each diffusing

Table II. **Brightness of GFP chimeras**

Sample	Count rate (kHz)/ molecule
GFP	0.95 (0.014)
PM-GFP	0.60 (0.022)
Gag-GFP	0.93 (0.024)
GagΔNC-GFP	0.73 (0.033)

Brightness of fluorescent species as determined by FCS. The values are the fluorescent count rates normalized by the concentration of molecules not associated with the membrane, as obtained from the amplitude of the correlation and the relative weighting of diffusion coefficients. The SEM is in parentheses. Average values are from $n = 10$ cells for each sample.

component is also determined from the autocorrelation curve, it is possible to measure the normalized brightness of molecules with a certain diffusion coefficient.

The values for counts per diffusing species were calculated for the cytosolic fractions of GFP, PM-GFP, Gag-GFP, and GagΔNC-GFP (Table II). This quantity is calculated using the fraction of species with diffusion coefficient of 10^{-3} μm^2/ms and greater, thereby explicitly rejecting the dominant diffusion peak associated with the membrane, as seen for example in PM-GFP (Fig. 7). The most significant feature of the normalized count rates is the absence of an overwhelming difference between Gag-GFP and the other moieties. If the large cytosolic diffusion coefficient were due entirely to aggregates of Gag in the cytoplasm, one would expect to see a 10–30-fold increase in brightness. Fluorescence quenching is likely to reduce the overall brightness of such a Gag aggregate, but the absence of any substantial increase in normalized count rates for Gag-GFP over the other fusion proteins suggests that these cytosolic aggregates do not consist of labeled Gag alone. The intermediate diffusing fluorescent species appear to represent at most a few Gag-GFP molecules bound to larger cellular complexes.

Detection of Gag containing complexes by subcellular fractionation

To provide independent evidence for the presence of large cytosolic complexes containing Gag protein, we performed [^{35}S]methionine steady-state or pulse-chase labeling of transfected cells expressing GagD37S (Fig. 8). After labeling, cells were lysed in hypotonic buffer in the absence of detergent, and the cytoplasmic fraction was submitted to rate-zonal sucrose gradient sedimentation. After steady-state labeling, the cytosolic GagD37S protein sedimented at three distinct locations in the gradient: one at the top (fraction 2 or 3), representing small oligomeric complexes; one in the middle (fraction 8), representing large complexes; and one at the bottom, possibly representing almost completely formed particles. As the chase time lengthened, the amount of Gag in both of the two complexes decreased, whereas the amount of Gag in the bottom fraction increased (Fig. 8 B).

Both of the two large complexes were disrupted by 0.5M NaCl (Fig. 8, A and C). To test if the Gag protein in fraction 2 represented monomeric protein, the sedimentation profile of GFP was determined by measuring the fluorescence intensity of each fraction of a parallel gradient. GFP, which is monomeric at this concentration, remained largely in the top fraction. The size difference between GagD37S (76kD) and GFP (29 kD) cannot explain the consistent one fraction shift in the gradient. We interpret the sedimentation pattern of Gag in high salt to represent a small oligomer of Gag, or a complex of Gag with a cellular protein.

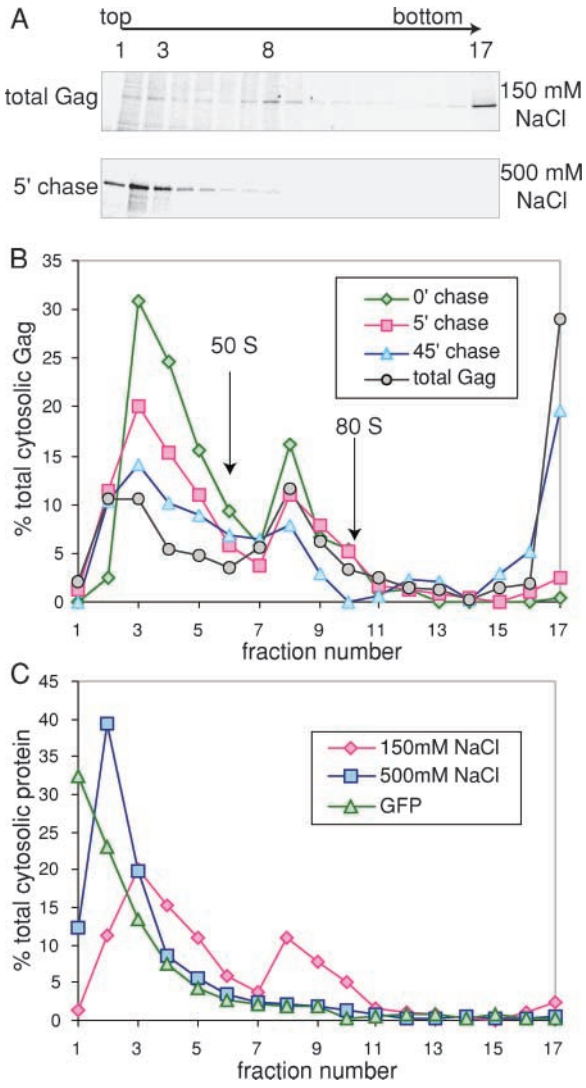

Figure 8. **Subcellular fractionation.** DF-1 cells transfected with DNA encoding GagD37S were pulse labeled or pulse-chase labeled with [^{35}S]methionine and lysed by homogenization after swelling of cells for 1 h in hypotonic buffer. Postnuclear supernatants were adjusted to 150 or 500 mM NaCl and submitted to rate zonal centrifugation on sucrose gradients at the same salt concentration. Each fraction was immunoprecipitated and the Gag protein was quantified by phosphorimaging. (A) Representative gel showing steady-state labeling (total Gag) or pulse labeling followed by a 5-min chase. The gradients were centrifuged at 50,000 rpm for 75 min. (B) Quantitation of Gag after centrifugation. The data from the top gel in A, and from parallel experiments (not depicted) were quantitated, with total radioactive Gag being normalized to 100%. The positions of purified 80 S ribosomes and 50 S ribosomal subunits were determined by spectrophotometry in parallel gradients. (C) Effect of high salt concentration on sedimentation. The positions of free GFP and of GagD37S were compared after centrifugation in 500 mM NaCl. The red curve is from B and is superimposed for comparison.

Discussion

Using implementations of two fluorescence techniques, two-photon FRET and FCS, we have addressed an important question in the field of retrovirus assembly in the RSV model system: Where in the cell do molecules of the viral structural protein, Gag, first interact with each other? We found that Gag-CFP and Gag-YFP proteins showed significant FRET not only at the plasma membrane at sites of assembly and budding but also in the cytoplasm, in equatorial sections of the whole cell, and in small focal volumes in the cytoplasm defined by 2PE. These results strongly suggest that Gag proteins interact in the cytoplasm before being transported to sites of assembly. Control experiments with a Gag mutant implicate the nucleic acid binding domain, NC, in these interactions, consistent with the known requirements for NC for assembly in vitro and in vivo (Bowzard et al., 1998; Cimarelli et al., 2000; Sandefur et al., 2000; Yu et al., 2001; Johnson et al., 2002). Thus, at least in the RSV system, it is likely that polymerization of the Gag shell occurs not by addition of monomeric Gag subunits, but instead by addition of dimeric or larger complexes. FCS measurements of diffusion of Gag-containing complexes in the cytoplasm suggest an approximate mass of ~10–100 MD. The fluorescence intensity of these complexes indicates the presence of only a few Gag molecules, implying that the complex is mostly cellular in origin. Sedimentation analysis of cell lysates confirms the existence of Gag complexes in the cytosol.

Several biochemical studies previously have implicated large Gag-containing complexes in assembly of HIV-1. One report provided evidence for two distinct complexes with density similar to authentic virus particles, one resistant to and one disrupted by detergents (Lee and Yu, 1998; Lee et al., 1999). NC was required for both. In another report, several putative assembly intermediates were identified in a coupled cell-free translation-assembly system, as well as in cells expressing HIV-1 Gag (Lingappa et al., 1997). The analysis used in both studies has several limitations. First, it is difficult to demonstrate that the Gag complexes are true assembly intermediates, because 80% of newly synthesized HIV Gag protein is reported to be degraded by proteasomes (Tritel and Resh, 2000). We found that all of the pulse-labeled RSV Gag protein eventually assembles and buds as VLPs, obviating this problem. Second, in subcellular fractionation, it is difficult to exclude formation of irrelevant complexes in the crude extract. Third, the reports on HIV-1 complexes do not distinguish between Gag–Gag interactions and Gag–cell protein interactions. Here, we avoid these problems by using two nonperturbative fluorescence techniques, which demonstrate direct Gag–Gag interaction with minimum manipulation of the cell.

FRET and FCS are complementary techniques for measuring intracellular Gag multimerization and trafficking. Both the whole cell FRET analysis and the inset analysis revealed strong FRET between donor and acceptor in regions of the cytoplasm where no punctate staining was visible. However, it is not possible to determine the extent of multimerization of Gag in the cytosol using FRET alone. FCS provides complementary information about multimerization of Gag: diffusion coefficients are a measure of aggregate size, and brightness provides an additional indication of multimerization. Furthermore, FCS can differentiate between membrane (including internal membranes) and cytosol, a distinction which is often difficult to make with imaging. Gag-GFP showed a diffusion peak intermediate between slow membrane bound diffusion and fast cytosolic diffusion. For this 3–10-fold change in diffusion, the mass would have to change by a factor of 30–1,000, according to the Stokes-Einstein equation. Although the Gag-GFP did display increased brightness in comparison to the GagΔNC-GFP, this increase was <50%. Together, the FRET and FCS measurements show that there is molecular interaction between Gag molecules in the cytosol, and that there are cellular complexes composed in part but not entirely of Gag.

There are several caveats for the interpretation of Gag diffusion coefficients in cells. The decrease of macromolecular mobility in the cytosol due to crowding is highly nonlinear with respect to the mass of the macromolecule (Verkman, 2002). Luby-Phelps and co-workers showed that when the mass of dye-labeled dextrans exceeds 500 kD, there is a sharp drop in cytosolic mobility (Luby-Phelps et al., 1986). Given the mass of Gag-GFP (97 kD), a Gag multimer containing ~5 or more Gag monomers would be sufficient to give the observed diffusion coefficient by this criteria. Although a "5mer" might not be sufficiently bright in the cytosol to observe with imaging, we would expect to observe close to a fivefold increase in the counts/molecule measured using FCS. The fact that we did not observe this dramatic increase argues that this intermediate diffusion coefficient is not due to aggregates of Gag alone. Other explanations for diffusion coefficients that are intermediate between those characteristic of the cytosol and of the membrane might be membrane flow or perhaps active transport along microtubules or microfilaments. However, the observation that labeled Gag molecules appeared to sediment with discrete S-values in sucrose gradients would argue against these possibilities.

The interaction between Gag and RNA appears to be the driving force for assembly of retroviral Gag proteins. Studies using in vitro systems have demonstrated that nucleic acid promotes formation of Gag dimers, which are inferred to be a key assembly intermediate (Yu et al., 2001; Ma and Vogt, 2002). Gag dimerization is also an essential step in vivo, as shown for Gag proteins with artificial dimerization domains substituted for NC (Zhang et al., 1998; Accola et al., 2000; Johnson et al., 2002). It seems likely that in vivo NC-RNA binding occurs first, leading to Gag–Gag interaction in cytoplasm, which then enables efficient membrane binding. The composition of the large cytosolic Gag complex inferred from FCS and from sedimentation analysis remains unknown.

Materials and methods

Plasmids

The starting plasmid was Gag-GFP, which is based on pGFP-N2 (CLONTECH Laboratories, Inc.) and has been described previously (Callahan and Wills, 2000). GagD37S and GagΔPR are nonfluorescent Gag molecules constructed by replacing the GFP fragment with the PR containing the active site mutation D37S, or by placing a stop codon immediately after the NC, respectively. For each fluorescent Gag protein, three versions with different GFP derivatives were constructed. CFP and YFP were amplified from CFP-C1 and YFP-C1 (CLONTECH Laboratories, Inc.) vectors. Gag-CFP and Gag-YFP were used for the FRET studies, whereas the GFP version was

used in the FCS measurements. The three GagΔMBD fluorescent proteins lack the first 83 aa in MA, and the three GagΔNC fluorescent proteins lack the entire 89 aa of NC.

Cell culture and transfection

The permanent chicken fibroblast cell line DF-1 was maintained in DME supplemented with 10% FBS and 1% vitamins. Transient transfections were performed by mixing plasmid DNA and Fugene reagent (Roche) as suggested by the manufacturer. For fluorescence studies, the cells were transferred to a glass bottom 35-mm dish (MatTek) 24 h after transfection and maintained in Leibovitz L-15 medium (GIBCO BRL) with the same supplementation for 12 h before microscopic analysis on a temperature controlled stage at 37°C. For FRET studies, 1 μg/dish each of the plasmid DNAs encoding Gag-CFP and Gag-YFP were cotransfected. The plasmid encoding PM-GFP, a GFP derivative engineered to contain the myristoylated and palmitylated NH_2-terminal sequence from the Lyn tyrosine kinase (Pyenta et al., 2001), was a gift from B. Baird (Cornell University, Ithaca, NY).

Metabolic labeling, immunoprecipitation and rate zonal gradient

DF-1 cells in 60-mm plates were labeled 24 h after transfection with 100 μCi of [^{35}S]methionine for 10 min in methionine-free medium (pulse) and were incubated further with unlabeled complete medium for various lengths of time (chase). To estimate budding efficiency, culture medium was collected and precleared by centrifugation at 1,500 *g* for 5 min. Virus particles were collected by centrifugation through a cushion of 15% sucrose in 20 mM Tris-HCl, pH 7.5, 100 mM NaCl, and 1 mM EDTA at 70,000 rpm in a TLA100.4 rotor (Beckman Coulter) for 20 min. The virus pellet was dissolved in SDS-PAGE sample buffer. To compare protein expression levels, transfected cells were lysed in ice-cold RIPA buffer (20 mM Tris-HCl, pH 7.5, 150 mM NaCl, 1% sodium deoxycholate, 1% Triton X-100, and 1 mM PMSF). Cell debris and nuclei were removed by centrifugation at 10,000 *g* for 5 min and immunoprecipitation was performed with anti-CA antiserum or anti-GFP antiserum (CLONTECH Laboratories, Inc.) as described previously in Schatz et al. (1997).

For rate zonal sedimentation analysis, DF-1 cells transfected with GagD37S were labeled with 300 μCi [^{35}S]methionine for 10 min and chased for various amounts of time, or continuously labeled for 1 h. The cells were then washed twice with ice-cold lysis buffer (1 mM Tris-HCl, pH 7.5, and 0.1 mM $MgCl_2$), scraped off from the plate in 250 μl lysis buffer and transferred to a microfuge tube followed by 1 h incubation on ice. The swollen cells were then lysed in a tissue homogenizer with a tight-fitting Teflon pestle. Nuclei, cell debris, and membranes were pelleted at 10,000 *g* for 10 min. The supernatant was loaded on a 4-ml 10–30% (wt/vol) gradient, which was made in buffer containing 25 mM Tris-HCl, pH 7.5, 1 mM EDTA, and 0.15 or 0.5 M NaCl. The gradient was centrifuged for 75 min at 50,000 rpm in a SW60 rotor (Beckman Coulter). Fractions were collected from the top of the gradient, diluted in 800 μl RIPA buffer, and immunoprecipitated with a mixture of anti–MA-p2 and anti-CA antibodies.

Two-photon microscopy and FCS

Imaging and FCS experiments were performed on a custom two-photon laser scanning microscope capable of laser scanning microscopy and stationary beam FCS. The excitation source was an ultrafast Ti:Sapphire Tsunami (Spectra-Physics). The beam was raster scanned at the sample with a MRC 600 scan box (Bio-Rad Laboratories) modified for near infrared excitation and coupled to an inverted microscope (model Axiovert 35; Carl Zeiss MicroImaging, Inc.) with a 63× C-Apochromat water objective (NA = 1.2; Carl Zeiss MicroImaging, Inc.). After the tube lens of the microscope, a 50-mm lens was used to collimate the emission. The emission was separated from the excitation with a 670 DCLP dichroic followed by an E800sp IR blocker. For FRET, the emission was then further separated with a 510 DCLP dichroic into a cyan channel (emission filter, HQ480/40 m) and a yellow channel (emission filter, HQ535/30 m). FCS measurements were performed using a single channel optimized for GFP (emission filter, HQ 575/150 m). All filters and dichroics were from Chroma Technology Corp. The detectors in both channels were GaAsP photon counting photomultipliers (Hamamatsu). Because 2PE provides intrinsic three dimensional resolution, no pinholes or apertures were used in the detection pathway. Correlation measurements were done with a 6010 Multiple Tau digital correlator (ALV).

The 830-nm excitation wavelength for the FRET experiment was chosen to maximize CFP absorption and minimize YFP absorption (Blab et al., 2001; Tsai et al., 2002). All FCS measurements were done with GFP, at an excitation wavelength of ~910 nm. In general, it is preferable to use long wavelengths (>900 nm) in cellular studies to reduce damage and minimize autofluorescence (Chen et al., 2002), and this wavelength is also near the peak of the GFP two-photon cross section (Heikal et al., 2001). Each curve was the average of five 10-s runs, resulting in a 50-s exposure to the cell. Only one curve was taken from each cell, with the error bars being the measured SD from the five runs. The average power in these FCS measurements was <2.5 mW.

FRET analysis

Due to the broad emission profiles of fluorescent proteins (Miyawaki et al., 1997; Tsien, 1998), there is significant overlap between donor emission and acceptor emission, resulting in spectral bleedthrough between fluorescence channels. To account for this bleedthrough, several correction schemes and analysis methods have been proposed (Miyawaki et al., 1997; Gordon et al., 1998; Xia and Liu, 2001; Erickson et al., 2001; Hoppe et al., 2002; Elangovan et al., 2003). The common aim of these methods is to generate a FRET image that is corrected for bleedthrough, expression levels, collection efficiency, background, and photobleaching, where each pixel is proportional to FRET efficiency.

We have implemented a methodology specifically designed to address the question of whether FRET occurs in the cytoplasm or at the plasma membrane. This method is based on z-series scans of cells in a culture dish and calculation of a FRET ratio at each z position. There is a greater fraction of plasma membrane at the ventral surface of the cell (in contact with the coverslip) and at the dorsal surface than in the equatorial regions of the cell. Therefore, a z-dependent FRET measurement can better distinguish between FRET contributions from the plasma membrane and the cytoplasm. Furthermore, this method does not attempt to generate a FRET image based on ratiometric approaches, which are inherently noisy when applied on a pixel-by-pixel basis. The approach described here is more robust, particularly in a cellular environment, but does not provide laterally resolved information.

All image analysis was done with IDL 5.4 (Research Systems, Inc.). The FRET ratio was calculated as the ratio of yellow intensity to cyan intensity within the cell for each plane of the z series. Thus, two images (cyan and yellow) at a single z position were reduced to one number, which reflects the amount of FRET, according to the following algorithm. First, the median of the image was subtracted to correct for the black level. Then, a binary mask was created by smoothing, choosing all points above a threshold, and finally using a gray scale closing operation. Once the binary mask was obtained, the original background-subtracted image was multiplied by the mask and summed. The net result of these manipulations was simply to define a region that constitutes the cell and to total the counts in that region. The ratio was obtained by dividing the value in the yellow channel by the value in the cyan channel. The same mask was used in both numerator and denominator. In a z-series acquisition, this operation was repeated at every plain of the z series for each set of images, yielding one ratio for each z step.

This method uses only a single excitation wavelength, namely the excitation maximum of the donor. We used this single excitation approach to eliminate the chromatic aberration effects and alignment artifacts, which are introduced by changing excitation wavelengths. The disadvantage of this method is that one cannot directly measure the acceptor concentration or account for direct excitation bleedthrough of the acceptor. However, the experimental results indicated that the acceptor was minimally excited at these wavelengths and that the donor fluorescence was the primary source of fluorescence bleedthrough (Results).

FCS analysis

FCS measures the fluorescence fluctuations resulting from diffusion of fluorescent entities into and out of an optically defined volume as a function of time. In this case, the volume is that in which 2PE occurs: ~1.2 μm in height and 0.5 μm in width. The concentration and the diffusion coefficient of the fluorescent species can be calculated from these data. The advantage of 2PE is the excellent registry between the recorded image and the positioning of the laser beam, enabling one to position the beam in the cell using the two-photon image as a guide. The autocorrelation function $G(\tau)$ is defined as:

$$G(\tau) = \frac{\langle \partial F(0) \partial F(\tau) \rangle}{\langle F(\tau) \rangle^2},$$

where $F(\tau)$ is the fluorescence obtained from the volume at delay time τ, brackets denote ensemble averages, and $\delta F(\tau) = F(\tau) - \langle F(\tau) \rangle$. The fitting formula is the standard fit for three dimensional multi-component diffusion (Thompson, 1991):

$$G(\tau) = \sum_i \frac{1}{N_i} \left(1 + \frac{4D_i\tau}{w_{xy}^2}\right)^{-1} \left(1 + \frac{4D_i\tau}{w_z^2}\right)^{-1/2},$$

where N_i is the number of species i; D_i is the diffusion coefficient of the i-th species; w_{xy} and w_z are the effective lateral and axial dimensions of the Gaussian focal volume, respectively.

This work was supported by National Science Foundation (NSF)–Science and Technology Center grant agreement no. ECS-9876771, National Center for Research Resources–National Institutes of Health (NIH) grant P41-RR04224, and NSF grant DBI-0080792 (to W.W. Webb); and NIH grant CA20081 (to V.M. Vogt).

Submitted: 31 March 2003
Accepted: 5 August 2003

References

Accola, M.A., B. Strack, and H.G. Gottlinger. 2000. Efficient particle production by minimal Gag constructs which retain the carboxy-terminal domain of human immunodeficiency virus type 1 capsid-p2 and a late assembly domain. *J. Virol.* 74:5395–5402.

Blab, G.A., P.H.M. Lommerse, L. Cognet, G.S. Harms, and T. Schmidt. 2001. Two-photon excitation action cross-sections of the autofluorescent proteins. *Chem. Physics. Lett.* 350:71–77.

Bowzard, J.B., R.P. Bennett, N.K. Krishna, S.M. Ernst, A. Rein, and J.W. Wills. 1998. Importance of basic residues in the nucleocapsid sequence for retrovirus Gag assembly and complementation rescue. *J. Virol.* 72:9034–9044.

Callahan, E.M., and J.W. Wills. 2000. Repositioning basic residues in the M domain of the Rous sarcoma virus gag protein. *J. Virol.* 74:11222–11229.

Campbell, S., and A. Rein. 1999. In vitro assembly properties of human immunodeficiency virus type 1 Gag protein lacking the p6 domain. *J. Virol.* 73: 2270–2279.

Campbell, S., and V.M. Vogt. 1997. In vitro assembly of virus-like particles with Rous sarcoma virus Gag deletion mutants: identification of the p10 domain as a morphological determinant in the formation of spherical particles. *J. Virol.* 71:4425–4435.

Chen, Y., J.D. Müller, Q. Ruan, and E. Gratton. 2002. Molecular brightness characterization of EGFP in vivo by fluorescence fluctuation spectroscopy. *Biophys. J.* 82:133–144.

Cimarelli, A., S. Sandin, S. Hoglund, and J. Luban. 2000. Basic residues in human immunodeficiency virus type 1 nucleocapsid promote virion assembly via interaction with RNA. *J. Virol.* 74:3046–3057.

Craven, R.C., and L.J. Parent. 1996. Dynamic interactions of the Gag polyprotein. *Curr. Top. Microbiol. Immunol.* 214:65–94.

Dayel, M.J., E.F.Y. Hom, and A.S. Verkman. 1999. Diffusion of green fluorescent protein in the aqueous-phase lumen of endoplasmic reticulum. *Biophys. J.* 76:2843–2851.

Denk, W., J.H. Strickler, and W.W. Webb. 1990. Two-photon laser scanning fluorescence microscopy. *Science.* 248:73–76.

Elangovan, M., H. Wallrabe, Y. Chen, R.N. Day, M. Barroso, and A. Periasamy. 2003. Characterization of one- and two-photon excitation fluorescence resonance energy transfer microscopy. *Methods.* 29:58–73.

Elson, E., and D. Magde. 1974. Fluorescence correlation spectroscopy. I. Conceptual basis and theory. *Biopolymers.* 13:1–27.

Erickson, M.G., B.A. Alseikhan, B.Z. Peterson, and D.T. Yue. 2001. Preassociation of calmodulin with voltage-gated Ca^{2+} channels revealed by FRET in single living cells. *Neuron.* 31:973–985.

Gordon, G.W., G. Berry, X.H. Liang, B. Levine, and B. Herman. 1998. Quantitative fluorescence resonance energy transfer measurements using fluorescence microscopy. *Biophys. J.* 74:2702–2713.

Gottlinger, H.G. 2001. The HIV-1 assembly machine. *AIDS.* 15(Suppl 5):S13–S20.

Gross, I., H. Hohenberg, and H.G. Krausslich. 1997. In vitro assembly properties of purified bacterially expressed capsid proteins of human immunodeficiency virus. *Eur. J. Biochem.* 249:592–600.

Heikal, A.A., S.T. Hess, and W.W. Webb. 2001. Multiphoton molecular spectroscopy and excited state dynamics of enhanced green fluorescent protein (EGFP): acid-base specificity. *Chem. Phys.* 274:37–55.

Hermida-Matsumoto, L., and M.D. Resh. 2000. Localization of human immunodeficiency virus type 1 Gag and Env at the plasma membrane by confocal imaging. *J. Virol.* 74:8670–8679.

Hess, S.T., S. Huang, A.A. Heikal, and W.W. Webb. 2002. Biological and chemical applications of fluorescence correlation spectroscopy: a review. *Biochemistry.* 41:697–705.

Hoppe, A., K. Christensen, and J.A. Swanson. 2002. Fluorescence resonance energy transfer-based stoiciometry in living cells. *Biophys. J.* 83:3652–3664.

Johnson, M.C., H.M. Scobie, Y.M. Ma, and V.M. Vogt. 2002. Nucleic acid-independent retrovirus assembly can be driven by dimerization. *J. Virol.* 76: 11177–11185.

Kingston, R.L., N.H. Olson, and V.M. Vogt. 2001. The organization of mature Rous sarcoma virus as studied by cryoelectron microscopy. *J. Struct. Biol.* 136:67–80.

Klikova, M., S.S. Rhee, E. Hunter, and T. Ruml. 1995. Efficient in vivo and in vitro assembly of retroviral capsids from Gag precursor proteins expressed in bacteria. *J. Virol.* 69:1093–1098.

Lee, Y.M., and X.F. Yu. 1998. Identification and characterization of virus assembly intermediate complexes in HIV-1-infected CD^{4+} T cells. *Virology.* 243:78–93.

Lee, Y.M., B. Liu, and X.F. Yu. 1999. Formation of virus assembly intermediate complexes in the cytoplasm by wild-type and assembly-defective mutant human immunodeficiency virus type 1 and their association with membranes. *J. Virol.* 73:5654–5662.

Lingappa, J.R., R.L. Hill, M.L. Wong, and R.S. Hegde. 1997. A multistep, ATP-dependent pathway for assembly of human immunodeficiency virus capsids in a cell-free system. *J. Cell Biol.* 136:567–581.

Luby-Phelps, K., D.L. Taylor, and F. Lanni. 1986. Probing the structure of the cytoplasm. *J. Cell Biol.* 102:2015–2022.

Ma, Y.M., and V.M. Vogt. 2002. Rous sarcoma virus gag protein-oligonucleotide interaction suggests a critical role for protein dimer formation in assembly. *J. Virol.* 76:5452–5462.

Magde, D., E. Elson, and W.W. Webb. 1972. Thermodynamic fluctuations in a reacting system. Measurement by fluorescence correlation spectroscopy. *Phys. Rev Lett.* 29:705–708.

Miyawaki, A., J. Llopis, R. Heim, J.M. McCaffery, J.A. Adams, M. Ikura, and R.Y. Tsien. 1997. Fluorescent indicators for Ca^{2+} based on green fluorescent proteins and calmodulin. *Nature.* 388:882–887.

Morikawa, Y., S. Hinata, H. Tomoda, T. Goto, M. Nakai, C. Aizawa, H. Tanaka, and S. Omura. 1996. Complete inhibition of human immunodeficiency virus Gag myristoylation is necessary for inhibition of particle budding. *J. Biol. Chem.* 271:2868–2873.

Niv, H., O. Gutman, Y.I. Henis, and Y. Kloog. 1999. Membrane Interactions of a constitutively active GFP-Ki-Ras 4B and their role in signaling. *J. Biol. Chem.* 274:1606–1613.

Periasamy, A. 2001. Fluorescence resonance energy transfer microscopy: a mini review. *J. Biomed. Opt.* 6:287–291.

Pyenta, P.S., D. Holowka, and B. Baird. 2001. Cross-correlation analysis of inner-leaflet-anchored green fluorescent protein co-redistributed with IgE receptors and outer leaflet lipid raft components. *Biophys. J.* 80:2120–2132.

Sandefur, S., V. Varthakavi, and P. Spearman. 1998. The I domain is required for efficient plasma membrane binding of human immunodeficiency virus type 1 Pr55Gag. *J. Virol.* 72:2723–2732.

Sandefur, S., R.M. Smith, V. Varthakavi, and P. Spearman. 2000. Mapping and characterization of the N-terminal I domain of human immunodeficiency virus type 1 Pr55(Gag). *J. Virol.* 74:7238–7249.

Schatz, G., I. Pichova, and V. Vogt. 1997. Analysis of cleavage site mutations between the NC and PR Gag domains of Rous sarcoma virus. *J. Virol.* 71:444–450.

Sekar, R.J., and A. Periasamy. 2003. Fluorescence resonance energy transfer (FRET) microscopy imaging of live cell protein localizations. *J. Cell Biol.* 160:629–633.

Thompson, N.L. 1991. Fluorescence correlation spectroscopy. *In* Topics in Fluorescence Microscopy. Vol. 1. J. Lakowiez, editor. Plenum Press, New York. 337–378.

Tritel, M., and M.D. Resh. 2000. Kinetic analysis of human immunodeficiency virus type 1 assembly reveals the presence of sequential intermediates. *J. Virol.* 74:5845–5855.

Tsai, P.S., N. Nishimura, E.J. Yoder, A. White, E. Dolnick, and D. Kleinfeld. 2002. Principles, design and construction of a two photon scanning microscope for in vitro and in vivo studies. *In* Methods for In Vivo Optical Imaging. R. Frostif, editor. CRC Press, Boca Raton, FL. 113–171.

Tsien, R.Y. 1998. The green fluorescent protein. *Annu. Rev. Biochem.* 67:509–544.

Verkman, A.S. 2002. Solute and macromolecule diffusion in cellular aqueous compartments. *Trends Biochem. Sci.* 27:27–33.

Vogt, V.M., and M.N. Simon. 1999. Mass determination of Rous sarcoma virus virions by scanning transmission electron microscopy. *J. Virol.* 73:7050–7055.

von Schwedler, U.K., T.L. Stemmler, V.Y. Klishko, S. Li, K.H. Albertine, D.R. Davis, and W.I. Sundquist. 1998. Proteolytic refolding of the HIV-1 capsid protein amino-terminus facilitates viral core assembly. *EMBO J.* 17:1555–1568.

Wills, J.W., and R.C. Craven. 1991. Form, function, and use of retroviral gag proteins. *AIDS.* 5:639–654.

Wills, J.W., R.C. Craven, R.A. Weldon, Jr., T.D. Nelle, and C.R. Erdie. 1991. Suppression of retroviral MA deletions by the amino-terminal membrane-binding domain of p60src. *J. Virol.* 65:3804–3812.

Xia, Z., and Y. Liu. 2001. Reliable and global measurement of fluorescence resonance energy transfer using fluorescence microscopes. *Biophys. J.* 81:2395–2402.

Yu, F., S.M. Joshi, Y.M. Ma, R.L. Kingston, M.N. Simon, and V.M. Vogt. 2001. Characterization of Rous sarcoma virus Gag particles assembled in vitro. *J. Virol.* 75:2753–2764.

Zhang, Y., H. Qian, Z. Love, and E. Barklis. 1998. Analysis of the assembly function of the human immunodeficiency virus type 1 gag protein nucleocapsid domain. *J. Virol.* 72:1782–1789.

Zhou, W., and M.D. Resh. 1996. Differential membrane binding of the human immunodeficiency virus type 1 matrix protein. *J. Virol.* 70:8540–8548.